PROCEEDINGS OF SPIE

SPIEDigitalLibrary.org/conference-proceedings-of-spie

Fabricate anti-solvent free tin-lead based perovskite solar cells with MAAc additives

C. Howlader, B. Mishra, N. Khakurel, D. Amyx, W. Geerts, et al.

C. Q. Howlader, B. Mishra, N. Khakurel, D. W. Amyx, W. Geerts, G. Gibson, M. Chen, "Fabricate anti-solvent free tin-lead based perovskite solar cells with MAAc additives," Proc. SPIE 12209, Organic, Hybrid, and Perovskite Photovoltaics XXIII, 1220905 (3 October 2022); doi: 10.1117/12.2634371



Event: SPIE Organic Photonics + Electronics, 2022, San Diego, California, United States

Fabricate anti-solvent free tin-lead based perovskite solar cells with MAAc additives

C. Q. Howlader*¹, B. Mishra¹, N. Khakurel¹, D.W. Amyx³, W. Geerts^{1,3}, G. Gibson⁴, and M. Chen^{1,2}
¹Material Science, Engineering, and Commercialization, Texas State University, TX 78666, USA;
²Ingram School of Engineering, Texas State University, San Marcos, TX 78666, USA; ³Department of Physics, Texas State University, San Marcos, TX 78666, USA; ⁴FAS Holdings Group, dba nTact, Dallas, TX 75238

ABSTRACT

Anti-solvent-free one-step deposition of perovskite thin film shows promising potential for application in slot-die or roll-to-roll mass-fabrication processes of perovskite solar cells. The continuous coverage was confirmed by PV response of devices made using the one-step deposition process. In this work, we have developed a process to deposit MAPb_{0.75}Sn_{0.25}($I_{0.5}$ Br_{0.5})₃ perovskite thin films without anti-solvent adding MAAc to the ink. By varying the Br content of the perovskite precursor, we were able to tune the bandgap. Fabricated solar cells with the structure ITO/CuI/ MAPb_{0.75}Sn_{0.25}($I_{0.5}$ Br_{0.5})₃ /C₆₀/BCP/Al with PCE of 4.59% show the path of the fabrication process of antisolvent-free tin-lead-based solar cells.

Keywords: Perovskite, anti-solvent-free, roll-to-roll, tin-lead, MAAc, bandgap

1. INTRODUCTION

Hybrid perovskite solar cells have shown immense progress within a very short time in term of efficiency. Kojima reported an efficiency of 3.81% in 20091 while as of 2022 single junction perovskite cells with efficiencies up to 25.7% are reported². Today's perovskite efficiencies are very comparable to that of single crystalline silicon (Si) solar cells². The perovskite structure is commonly represented by ABX3, where A is a monovalent cation, B is a divalent metal cation, and X are halide ions. MAPbI₃ (CH₃NH₃PbI₃) is the most explored perovskite material. Its bandgap is a good match for the solar spectrum resulting in high efficiency devices³. However, in recent years, there are raising concerns regarding the toxicity of the organic inorganic hybrid perovskite solar cells^{4,5}. Using lead in perovskite solar cells makes perovskite solar cells questionable to be used as green energy sources. Thus, it's necessary to replace the lead with another compatible material. Several materials have been explored to replace Pb in perovskites including bismuth (Bi), antimony (Sb), germanium (Ge) and tin (Sn). Among them Sn is the most suitable material to replace lead in the perovskite structure enabling realization of devices with efficiencies of over 19%⁴. As completely tin-based perovskite suffers from poor power conversion efficiency (PCE) compared to its counterparts' lead-based perovskite solar cells, researchers are more interested in tin-lead binary perovskites. These materials have improved PCE, stability⁶, as well as enable bandgap tuning to optimize the energy harvesting wavelength. A binary tin-lead perovskite CH₃NH₃Sn_{0.5}Pb_{0.5}I₃ with bandgap of 1.18 eV was utilized for the first time by Y. Ogomi et al. to realize 4.18% PCE devices⁷. Although single junction solar cells have a limit of power conversion efficiency according to Shockley- Queisser limit, efficiency can be increased by constructing multijunction solar cells and combining the perovskite layer with a traditional silicon solar cell. The high energy photons are absorbed by the top perovskite layer while the red and near infrared part of the spectrum is absorbed by the silicon. Such applications require perovskites with a wider bandgap, ideally 1.67 eV when used on top of a traditional silicon solar cell. Compositional engineering of the ABX₃ perovskite structure by for example using a mix of different halide ions can be used to tune the bandgap to make it suitable for such tandem solar cells. Promise to include Sn-based perovskites in multijunction cells was shown by Z. Yang et al. They demonstrated that the bandgap of Sn_{0.25}Pb_{0.75}-based perovskite can be tuned by varying the ratio of Br and I. Their MAPb_{0.75}Sn_{0.25}(I_{0.4}Br_{0.6})₃ devices with a 1.73 eV bandgap had an efficiency of 12.59% and are promising for tandem cells on silicon8. The same group also reported on MAPb_{0.5}Sn_{0.5}(I_{0.8}Br_{0.2})₃ devices (lower bandgap interesting for single junction devices) with an efficiency of 17.63% 9. They also reported that the incorporation of Br in the perovskite structure can improve the film qualities in different ways such as lower nonradiative

Organic, Hybrid, and Perovskite Photovoltaics XXIII, edited by Gang Li, Natalie Stingelin, Proc. of SPIE Vol. 12209, 1220905 ⋅ © 2022 SPIE 0277-786X ⋅ doi: 10.1117/12.2634371

^{*}Chandan.howlader@txstate.edu; phone 1 512 210 - 7312

recombination rate, and other advantages related to band edge disorder and Urbach energy coupled with higher absorption coefficient. Z. Zhu et al. utilized galvanic the displacement approach to improve the PCE of FA_{0.85}MA_{0.15}Pb_{0.6}Sn_{0.4}(I_{0.85}Br_{0.15})₃ to 18.21 % with ambient and thermal stability in encapsulation ¹⁰. Further improvement of PCE to 19 % was obtained by C. Li et al. by incorporating a small amount of Br in the MASn_{0.6}Pb_{0.4}I₃ reducing the bandgap to 1.27eV ¹¹. Most of the published works show different approaches to improve the efficiency of the solar cell with one common practice, i.e use anti-solvent while spin coating the perovskite thin film. Anti-solvent is normally used to induce a homogeneous nucleation distribution to avoid a nonuniform film with lots of pinholes. Note that tin-lead binary perovskite has the tendency to rapidly growth while depositing. As anti-solvent is not a suitable process step to include in a mass fabrication process such as slot-die printing or roll-to-roll processes, here we developed a process to deposit binary perovskite thin films without anti-solvent step. By using Methylammonium acetate (MAAc) additive in the ink, the nucleation and growth was modified resulting in continuous pin-hole free spin casted films. In order to demonstrate the pin hole free method, the absorber layer was incorporated in solar cells devices using the structure of ITO/CuI/MAPb_{0.75}Sn_{0.25}(I_{0.50}Br_{0.50})₃/C60/BCP/Al.

2. EXPERIMENTAL DESCRIPTION

2.1 Ink preparation:

The ink for the CuI hole transport layer was prepared by dissolving 30 mg of commercially available copper iodide (Sigma Aldrich) in 1 ml of acetonitrile (Millipore Sigma). The mixture was stirred at room temperature (RT) at 550 rpm for 45 min. After this procedure the solution was filtered using a 0.45 µm PTFE filter before use.

The perovskite MAPb_{0.75}Sn_{0.25}(I_{0.50}Br_{0.50})₃ ink was made using commercially available chemicals purchased from Alpha Aesar and Sigma Aldrich. To prepare the Sn-Pb precursor solution, 50 mol% methylammonium iodide (MAI), 50 mol% methylammonium bromide (MABr), 37.5 mol% lead (II) iodide (PbI₂), 37.5 mol% lead (II) bromide (PbBr₂), 12.5 mol% tin (II) iodide (SnI₂) and 12.5 mol% tin (II) bromide (SnBr₂) were dissolved in 1 ml of DMF solvent and stirred at 550 rpm on a hot plate at 70° C for 1 hour. After that 100 mol% of MAAc were added to the ink and let it dissolve at RT for 20 min. The ink was filtered using a 0.22 μm PTFE filter before use.

2.2 Device fabrication:

Commercially available prepatterned ITO substrates were cleaned for 20 minutes by ultrasonication in 5% Deconex in DI water followed by ultrasonically cleaning for 20 minutes in DI water. Cleaned substrates were dried with nitrogen gas followed by additional cleaning in an air plasma (300 Watt) for 10 minutes. The samples were loaded in a nitrogen glovebox. Around 100 μ l of CuI was dispensed on the ITO substrate which was spun at 2000 rpm for 60s and then dried at 150 °C for 15 min. Before depositing the perovskite precursor, the sample was cooled down for 45 min. Then 85 μ l of perovskite precursor ink was dispensed onto the ITO/CuI and spun at 6000 rpm for 60s and dried at 110 °C for 10 min. Patterning of the perovskite was done by removing the film at specific areas using and X-acto knife. The C₆₀ (40 nm)/BCP (8 nm)/Al (100 nm) stack were deposited sequentially by thermal evaporator through deposition masks. Figure 1 shows the schematic diagram of fabricated solar cells. Each wafer contains four devices that each have an area of ~0.0625cm². Finally, the solar cells were encapsulated inside the glove box using an encapsulation robot.

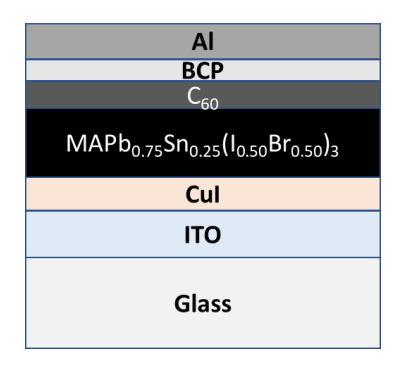


Figure 1: Schematic diagram of the fabricated device structure.

2.3 Sample characterization:

The different layer of the device were also deposited separately on glass or ITO substrates and characterized by different tools to determine the physical and optical properties. Θ -20 XRD spectra were measured by a Rigaku SmartLab X-ray Diffractometer (XRD) with Cu target at 40 KeV. SEM pictures were taken by a FEI Helios NanoLab 400 DualBeam SEM with ETD. Topographic AFM pictures were taken by a Bruker Dimension ICON AFM using the HQ:NSC15/Al BS tip. AFM images were analyzed by Gwyddion software to determine the roughness. Thicknesses were measured using a KLA Tencor P7 stylus profilometer. UV-Vis spectra were measured using a Shimadzu UV-2600 spectrometer to determine the absorption spectra.

2.4 Device characterization:

Electrical performance of the solar cells was characterized using an Oriel ABA sun simulator with an AM 1.5G filter installed. Devices were tested under $1 sun (100 mW/cm^2)$ illumination. The sample was connected to a Keithley 2400 source meter to measure current density (I) versus applied voltage (V) from -0.1 V to 1.1 V. A LabView program was used to log the current and voltage and calculate the solar cell parameters including PCE, open circuit voltage (V_{OC}), short circuit current (I_{SC}) and fill factor (FF).

3. RESULT AND DISCUSSION

Nonuniform, fast and uncontrollable growth of the perovskite leads to rough surfaces and interfaces and pinholes in the perovskite thin film¹². Inducing a homogeneous high nucleation density and slowing down the growth process is a commonly practiced technique to get a fully covered thin film. This can be done by additive engineering. For instance, MAAc in MAPI perovskite ink has a positive impact on the nucleation and growth during deposition and results in a pinhole free thin film deposition with excellent photovoltaic performance¹³. MAAc in the precursor solution introduces an intermediate phase and exchange between X- anion of MA+X- and Ac- anion of the intermediate phase create perovskite structure¹⁴. As the MAAc evaporates during the curing process it does not stay in the film. Here we explore if this formation process could also be applied to the deposition of a Sn-Pb binary perovskite film. Our previous experiment showed that incorporating more than 50 mol% of MAAc in the perovskite precursor is enough to get a pinhole free film¹⁵. Figure 1 a) shows the Scanning electron microscopy (SEM) image of a perovskite film casted with ink containing 100 mol% of MAAc concentration. It is clear from the image that the film is uniform and does not have any pinholes.

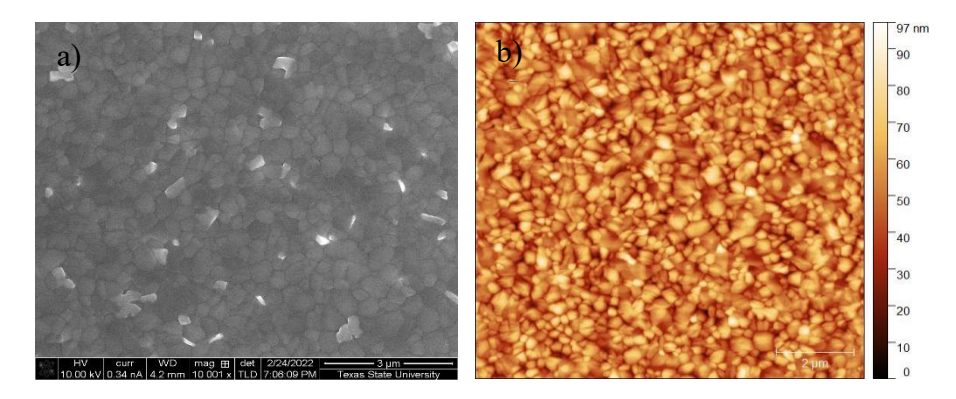


Figure 2: a) SEM and b) AFM image of MAPb_{0.75}Sn_{0.25}(I_{0.5}Br_{0.5})₃ perovskite thin film with 100 mol% of MAAc.

Film morphology was determined by the atomic force microscopy (AFM), which is shown in figure 1 b). Roughness of the film is determined around \sim 10 nm and the thickness around \sim 210 nm. Also, the film was characterized by X-ray diffraction to determine the phase ID before and after annealing.

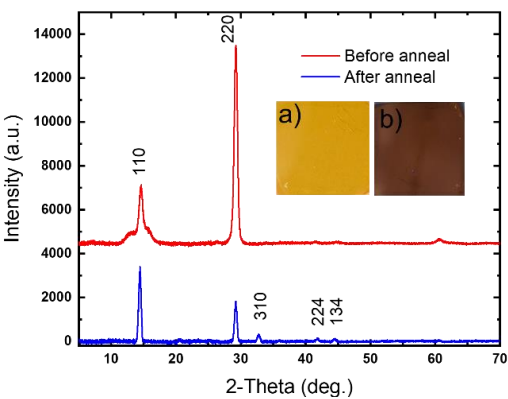


Figure 3: XRD spectra of MAPb_{0.75}Sn_{0.25}(I_{0.5}Br_{0.5})₃ perovskite before and after annealing. Inset pictures are optical images a) before and b) after annealing.

Figure 3 shows the XRS spectra of the thin film before annealing (Top spectra) and this film shows a strong dominance of 220 orientation. There is also another orientation along 110. Inset optical pictures of figure 3 shows the color of the film a) before and b) after annealing. Note that the colors are completely different suggesting a different electronic structure. After annealing the dominating orientation is changed to 110. Also, there are some other minor orientations of crystalline structure observed.

The bandgap of the film can be determined from the absorption edge. To examine the bandgap tunability of this binary perovskite, we changed the bromine and iodine ratio in the precursor and checked the absorption spectra. Figure 4 shows the absorption spectra of MAPb_{0.75}Sn_{0.25}(I_{1-x}Br_x)₃ perovskite. The bandgap increases linearly with the increase of the bromine content in the perovskite solution. For the X value of 0, 0.25, 0.5, 0.75, and 1, we determined the corresponding bandgap to be 1.31 eV, 1.41 eV, 1.61 eV, 1.73 eV, and 1.92eV respectively. From this, we choose to use 1.61 eV bandgap to check the photovoltaic properties of MAAc assisted binary perovskite.

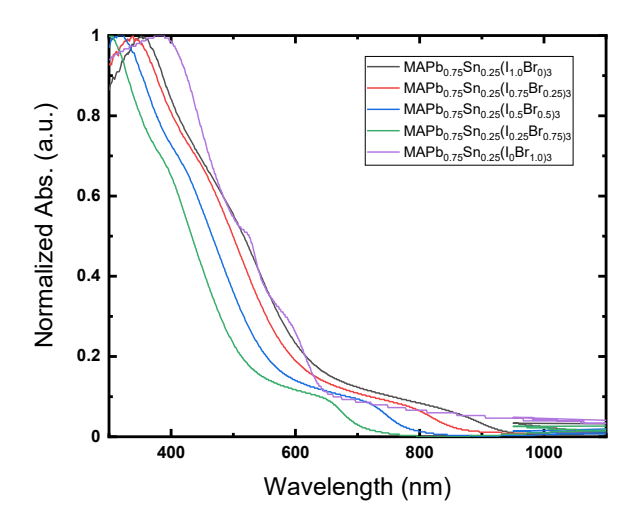


Figure 4: UV-Vis spectra of MAPb_{0.75}Sn_{0.25}(I_xBr_{1-x})₃ perovskite

We have fabricated solar cells using the MAAC assisted binary perovskite absorber layer. Figure 5 shows the I-V curve of the fabricated solar cells with the structure of Glass/ITO/CuI/CH₃NH₃Pb_{0.75}Sn_{0.25}(I_{0.5}Br_{0.5})₃/C₆₀/BCP/Al. From the I-V measurement we obtained a PCE of 4.59%, Voc is 0.67 V, Isc is 13.14 mA and the fill factor is 52.52%. Note that the device has a clear PV signal which indicates that the absorber layer is indeed continuous and pinhole free. The efficiency observed is below that of Yang et al, who used a similar device structure but instead of the CuI used PEDOT:PSS.

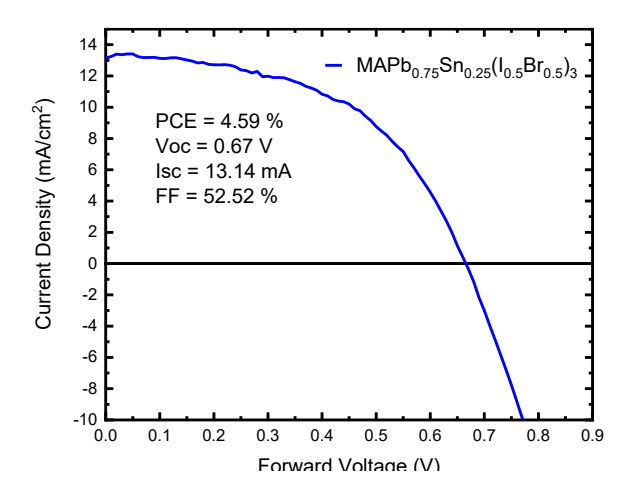


Figure 5: I-V curves for MAPb_{0.75}Sn_{0.25}(I_{0.5}Br_{0.5})₃ perovskite solar cells.

The lower performance of the solar cell can be described by the high series and low shunt resistance. Also there are other factors could perticipate in the poor PCE such as ion migration between grain boundaries, impurities in the materials, and oxidation of the Sn to enhance the recombination mechanism ^{16,17}.

4. CONCLUSION

We have successful demonstrated the deposition process of pinhole-free $CH_3NH_3Pb_{0.75}Sn_{0.25}(I_{0.5}Br_{0.5})_3$ with MAAc additives engineering. It was also shown that the additives do not change the film's optical properties. Finally, we can say that it is a path to fabricate tin-lead based solar cells without anti-solvent in a one-step deposition process for mass fabrication. Fabricated solar cells show a PCE of 4.59 % with 52.52 % of FF, 13.14 mA I_{sc} and 0.67 V V_{oc} .

5. ACKNOWLEDGEMENTS:

This work was in part funded by the Department of Navy's HBCU/MI Program through ONR grant **number** N00014-19-1-2576 and in part by NSF through SBIR Phase II grant 1927020.

REFERENCES

- [1] Kojima, A., Teshima, K., Shirai, Y. and Miyasaka, T., "Organometal halide perovskites as visible-light sensitizers for photovoltaic cells," J. Am. Chem. Soc. **131**(17), 6050–6051 (2009).
- [2] Laboratory, N. R. E., "Best research-cell efficiency chart" (2022)," https://www.nrel.gov/pv/cell-efficiency.html.
- [3] Cao, J., Loi, H. L., Xu, Y., Guo, X., Wang, N., Liu, C. ki, Wang, T., Cheng, H., Zhu, Y., Li, M. G., Wong, W. Y. and Yan, F., "High-Performance Tin–Lead Mixed-Perovskite Solar Cells with Vertical Compositional Gradient," Adv. Mater. **34**(6), 1–10 (2022).
- [4] Li, Y., Sun, W., Yan, W., Ye, S., Rao, H., Peng, H., Zhao, Z., Bian, Z., Liu, Z., Zhou, H. and Huang, C., "50% Sn-Based Planar Perovskite Solar Cell with Power Conversion Efficiency up to 13.6%," Adv. Energy Mater. **6**(24) (2016).
- [5] Howlader, C., Hasan, M., Zakhidov, A. and Chen, M. Y., "Determining the refractive index and the dielectric constant of PPDT2FBT thin film using spectroscopic ellipsometry," Opt. Mater. (Amst). **110**(October), 110445 (2020).
- [6] Liu, Y., Gao, W., Ran, C., Dong, H., Sun, N., Ran, X., Xia, Y., Song, L., Chen, Y. and Huang, W., "All-

- inorganic Sn-based Perovskite Solar Cells: Status, Challenges, and Perspectives," ChemSusChem 13(24), 6477–6497 (2020).
- [7] Ogomi, Y., Morita, A., Tsukamoto, S., Saitho, T., Fujikawa, N., Shen, Q., Toyoda, T., Yoshino, K., Pandey, S. S., Ma, T. and Hayase, S., "CH3NH3SnxPb(1-x)I3 perovskite solar cells covering up to 1060 nm," J. Phys. Chem. Lett. **5**(6), 1004–1011 (2014).
- [8] Yang, Z., Rajagopal, A., Jo, S. B., Chueh, C. C., Williams, S., Huang, C. C., Katahara, J. K., Hillhouse, H. W. and Jen, A. K. Y., "Stabilized Wide Bandgap Perovskite Solar Cells by Tin Substitution," Nano Lett. **16**(12), 7739–7747 (2016).
- [9] Yang, Z., Rajagopal, A. and Jen, A. K. Y., "Ideal Bandgap Organic-Inorganic Hybrid Perovskite Solar Cells," Adv. Mater. **29**(47), 1–7 (2017).
- [10] Zhu, Z., Li, N., Zhao, D., Wang, L. and Jen, A. K. Y., "Improved Efficiency and Stability of Pb/Sn Binary Perovskite Solar Cells Fabricated by Galvanic Displacement Reaction," Adv. Energy Mater. 9(7) (2019).
- [11] Li, C., Song, Z., Zhao, D., Xiao, C., Subedi, B., Shrestha, N., Junda, M. M., Wang, C., Jiang, C. S., Al-Jassim, M., Ellingson, R. J., Podraza, N. J., Zhu, K. and Yan, Y., "Reducing Saturation-Current Density to Realize High-Efficiency Low-Bandgap Mixed Tin–Lead Halide Perovskite Solar Cells," Adv. Energy Mater. 9(3), 1–9 (2019).
- [12] Ghosh, S., Mishra, S. and Singh, T., "Antisolvents in Perovskite Solar Cells: Importance, Issues, and Alternatives," Adv. Mater. Interfaces 7(18), 1–24 (2020).
- [13] Xia, Y., Ran, C., Chen, Y., Li, Q., Jiang, N., Li, C., Pan, Y., Li, T., Wang, J. P. and Huang, W., "Management of perovskite intermediates for highly efficient inverted planar heterojunction perovskite solar cells," J. Mater. Chem. A 5(7), 3193–3202 (2017).
- [14] Xiao, Y., Yang, L., Han, G., Li, Y., Li, M. and Li, H., "Effects of methylammonium acetate on the perovskite film quality for the perovskite solar cell," Org. Electron. **65**, 201–206 (2019).
- [15] Howlader, C. Q., Khakurel, N., Amyx, D. W., Geerts, W., Gibson, G. and Chen, M., "Pin-hole free MAPb0.75 Sn0.25(I0.5Br0.5)3 films spin casted without anti-solvent by adding MAAc additive to Perovskite ink," 0–4 (2022).
- [16] Swartz, C. H., Khakurel, N., Najar, S. R., Hossain, M. I. and Zakhidov, A., "Temperature- and Bias-Dependent Degradation and Regeneration of Perovskite Solar Cells with Organic and Inorganic Hole Transport Layers," Phys. Status Solidi Appl. Mater. Sci. **218**(7), 1–9 (2021).
- [17] Chen, B., Yang, M., Priya, S. and Zhu, K., "Origin of J-V Hysteresis in Perovskite Solar Cells," J. Phys. Chem. Lett. 7(5), 905–917 (2016).